Pearlite in Ultrahigh Carbon Steels: Heat Treatments and Mechanical Properties

ERIC M. TALEFF, CHOL K. SYN, DONALD R. LESUER, and OLEG D. SHERBY

Two ultrahigh carbon steel (UHCS) alloys containing 1.5 and 1.8 wt pct carbon, respectively, were studied. These materials were processed into fully spheroidized microstructures and were then given heat treatments to form pearlite. The mechanical properties of the heat-treated materials were evaluated by tension tests at room temperature. Use of the hypereutectoid austenite-cementite to pearlite transformation enabled achievement of pearlitic microstructures with various interlamellar spacings. The yield strengths of the pearlitic steels are found to correlate with a predictive relation based on interlamellar spacing and pearlite colony size. Decreasing the pearlite interlamellar spacing increases the yield strength and the ultimate strength and decreases the tensile ductility. It is shown that solid solution alloying strongly influences the strength of pearlitic steels.

I. INTRODUCTION

ULTRAHIGH carbon steels (UHCS), which are hypereutectoid steels, have been a topic of much interest for their unique mechanical properties. Particularly of recent interest are the high strengths which UHCS materials exhibit. A majority of the studies concerning room-temperature strength in UHCS alloys have concentrated on fully spheroidized microstructures.[1,2] Another microstructural condition yielding interesting mechanical properties at room temperature is pearlite, which can be formed by heat treatment from a spheroidized microstructure. Because UHCS materials lie in the hypereutectoid region of the Fe-C phase diagram, the pearlite transformation is different from that in hypoeutectoid steels. In austenitizing unalloyed UHCS, the amount of carbon dissolved in austenite can be varied from the eutectoid composition of 0.77 wt pct at the A_1 temperature to a maximum of 2.1 wt pct at the A_{cm} temperature at the E point (the point of maximum solubility of carbon in austenite). Upon air cooling of UHCS below the A_1 temperature, austenite with dissolved carbon is converted into pearlite. As the amount of carbon dissolved in austenite is increased, fewer cementite particles will be retained from the original spheroidized microstructure and their sizes will be smaller. An increase in the amount of carbon dissolved in austenite prior to transformation will result in a decrease in the interlamellar spacing of the transformed pearlite. In austenite at or below the A_1 transformation temperature, an increase in dissolved carbon increases the driving force for pearlite formation, resulting in a decrease of the interlamellar spacing for nucleated pearlite. This process also allows for the creation of various ratios of spheroidized carbide to lamellar pearlitic carbide from an initially spheroidized microstructure.

The two alloys studied contain 1.5 wt pct C (UHCS-1.5C) and 1.8 wt pct C (UHCS-1.8C). Each alloy also contains 1.6 wt pct Al, 1.5 wt pct Cr, and 0.5 wt pct Mn. The addition of Mn minimizes the deleterious effects of sulfur and phosphorus. The addition of Cr helps to prevent graphitization and stabilizes the carbides, making coarsening more difficult. The addition of Al inhibits the formation of a hypereutectoid carbide network and stabilizes the ferrite phase. The addition of 1.6 wt pct Al raises the A_1 transformation temperature from 727 °C to approximately 780 °C. Figure 1 shows an approximation of the Fe-C phase diagram for alloys containing 1.6 wt pct Al, 1.5 wt pct Cr, and 0.5 wt pct Mn.[3] The two UHCS alloys of this study are denoted in Figure 1 by vertical lines at their respective carbon contents.

II. EXPERIMENTAL PROCEDURE

Each of the two UHCS materials was cast into an ingot and then hot-forged into bars of 51 × 51 mm cross section. Sections of 51-mm length were cut from each bar and processed by hot-and-warm working (HWW) into plates for making tensile samples. The HWW processing involves rolling the material from above the A_{cm} temperature until it reaches the A_1 temperature. This processing procedure substantially refines the microstructure. The UHCS-1.8C material was subsequently given a divorced-eutectoid transformation (DET) in order to fully spheroidize the microstructure. The DET involves heating just above the A_1 temperature and air cooling.[4] The UHCS-1.5C material was given a DET with associated deformation (DETWAD) treatment in order to create a spheroidized microstructure. The DETWAD involves heating slightly above the A_1 temperature, as in a DET, and rolling while cooling.[4] The results for both materials were fine, spheroidized carbide microstructures.

The processed plates of each material were machined into tensile coupons with gage lengths of 25.4 mm. Machined samples were sealed in stainless-steel bags for heat treatment. Powders of titanium were inserted into each bag

ERIC M. TALEFF, Assistant Professor, is with the Department of Aerospace Engineering and Engineering Mechanics, The University of Texas at Austin, Austin, TX 78712-1085. CHOL K. SYN, Engineer/Materials Scientist, and DONALD R. LESUER, Group Leader/Materials Engineer, are with the Manufacturing and Materials Engineering Division, Lawrence Livermore National Laboratory, Livermore, CA 94550. OLEG D. SHERBY, Professor, is with the Department of Materials Science and Engineering, Stanford University, Stanford, CA 94305.

Manuscript submitted January 9, 1995.

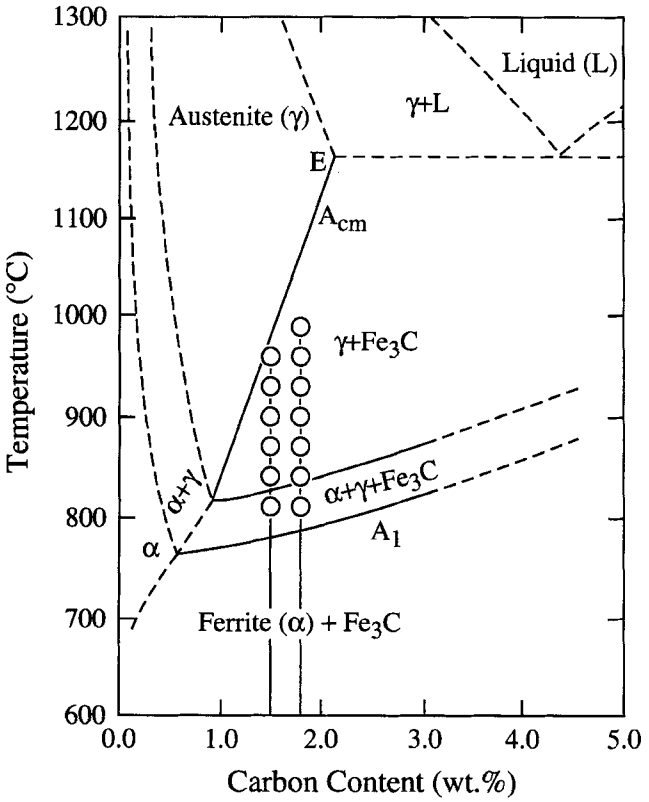

Fig. 1—An approximate phase diagram of the Fe-C system for alloys containing 1.6 wt pct Al, 1.5 wt pct Cr, and 0.5 wt pct Mn.[3] Open circles represent austenitizing temperatures selected in this study.

in order to absorb oxygen during heating and to prevent oxidation of the samples. Samples were austenitized for 20 to 30 minutes at temperatures between the A_1 and A_{cm} temperatures. Each sample was air cooled after austenitizing in order to form pearlite. Samples of UHCS-1.5C were austenitized at temperatures of 810 °C, 840 °C, 870 °C, 900 °C, 930 °C, and 960 °C. Samples of UHCS-1.8C were austenitized at temperatures of 810 °C, 840 °C, 870 °C, 900 °C, 930 °C, 960 °C, and 990 °C. The austenitizing temperatures for each material are indicated by open circles in the approximated phase diagram of Figure 1. The samples were tested in tension to failure, and strain was measured by an extensometer. After failure, microscopy samples were taken from the undeformed grip region of specimens from each heat treatment. Microscopy samples were etched with nital, given a conductive coating, and analyzed in a scanning electron microscope (SEM).

III. RESULTS

The microstructures resulting from each heat treatment in the UHCS-1.5C material are shown in Figure 2. Figures 2(a) through (f) show the effects of progressively higher austenitizing temperatures, from 810 °C for Figure 2(a) to 960 °C for Figure 2(f). These microstructures show an increase in the amount of pearlitic carbide and a decrease in the amount of spheroidized carbide with increasing austenitizing temperature. After austenitizing at 810 °C and air cooling, the microstructure is almost completely spheroidized because of the DET process (Figure 2(a)), and after austenitizing at 960 °C and air cooling, the microstructure is nearly all pearlite (Figure 2(f)). As the quantity of pearlitic carbide increases in comparison with spheroidized carbide, the pearlite interlamellar spacing decreases significantly. Because some spheroidized carbides remain undissolved during all austenitizing treatments below the A_{cm} line, grain growth is inhibited and a fine pearlite colony size is obtained after transformation. The microstructures resulting from each heat treatment of UHCS-1.8C are shown in Figure 3. Figure 3(a) shows the DET microstructure. Figures 3(b) through (h) show the transformed microstructures from austenitizing treatments at 810 °C (Figure 3(b)) through 990 °C (Figure 3(h)). The same trends observed in UHCS-1.5C are observed for the UHCS-1.8C material. The UHCS-1.8C material is fully spheroidized after the 810 °C heat treatment (Figure 3(b)) because of the DET process. After austenitizing at 990 °C, the microstructure is fully pearlitic with extremely fine interlamellar spacings (Figure 3(h)). The pearlite interlamellar spacings of each heat treatment for the UHCS-1.5C and UHCS-1.8C materials were measured from the finest observable interlamellar spacing under the SEM and are given in Table I. The pearlite colony sizes are also listed in Table I. For these two UHCS alloys, the pearlite colony size is considered effectively the same as the prior austenite grain size. The relationship between pearlite interlamellar spacing, λ, and austenitizing temperature is shown in Figure 4. Of note is the sharp initial drop in interlamellar spacing with increasing austenitizing temperature until fine spacings of less than 0.1 μm are reached.

Data from tensile tests of the heat-treated UHCS-1.5C samples are given in Figure 5 as a plot of engineering stress *vs* engineering strain. Of note is the maximum ductility of 15 pct obtained for the sample austenitized at 840 °C. Also of note are the very high yield and ultimate tensile strengths observed, with yield strengths of over 1000 MPa for the samples austenitized at 930 °C and 960 °C. Data from tensile tests of the heat-treated UHCS-1.8C samples are given in Figure 6 as a plot of engineering stress *vs* engineering strain. These data show a maximum ductility of between 13 and 14 pct for the samples austenitized at 810 °C and 840 °C. Remarkably high yield strengths of 1200 MPa are observed for the samples austenitized at 960 °C and 990 °C. Very high ultimate strengths are observed for both the UHCS-1.5C and UHCS-1.8C materials and are limited by fracture to a maximum value of 1600 MPa for the case of the sample austenitized at 990 °C.

IV. DISCUSSION

Yield strength was found to correlate well with the inverse square root of interlamellar spacing, λ. Figure 7 shows this good correlation on a plot of yield strength *vs* inverse square root of interlamellar spacing for both the UHCS-1.5C and UHCS-1.8C materials. The observed relationship has been used in other studies to describe pearlite strength and follows a Hall–Petch type relation, given as

$$\sigma_y = \sigma_0 + k_y \lambda^{-1/2} \quad [1]$$

where σ_y is the yield stress, σ_0 is the friction stress, k_y is a material constant, and λ is the interlamellar spacing. Data from Hyzak and Bernstein and from Gladman *et al.* on eutectoid steels also show strengths which vary linearly

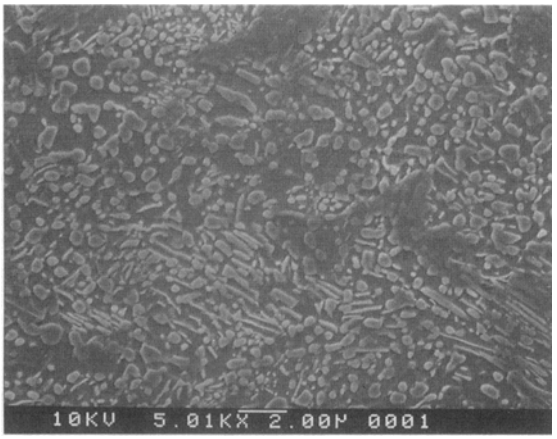

(*a*)

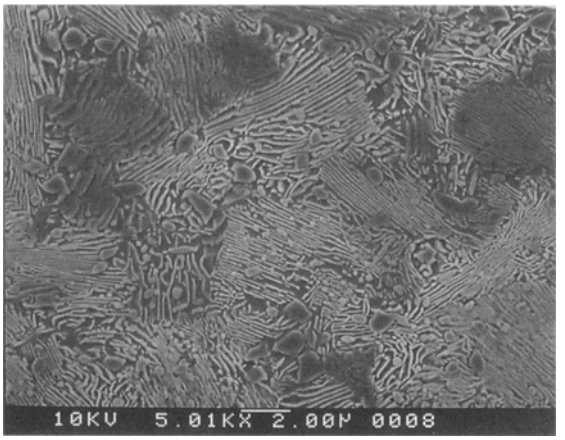

(*d*)

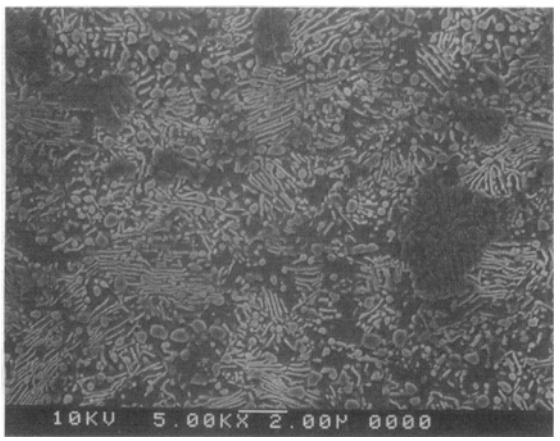

(*b*)

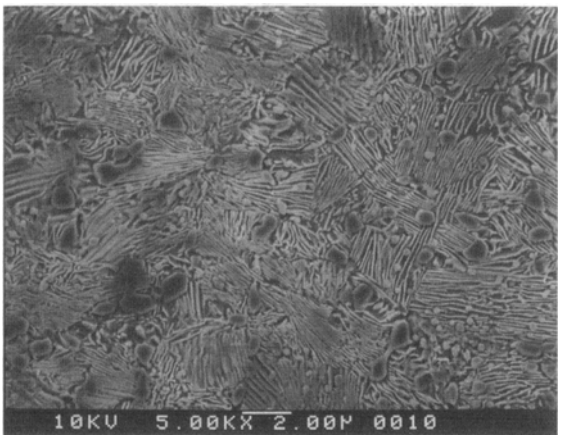

(*e*)

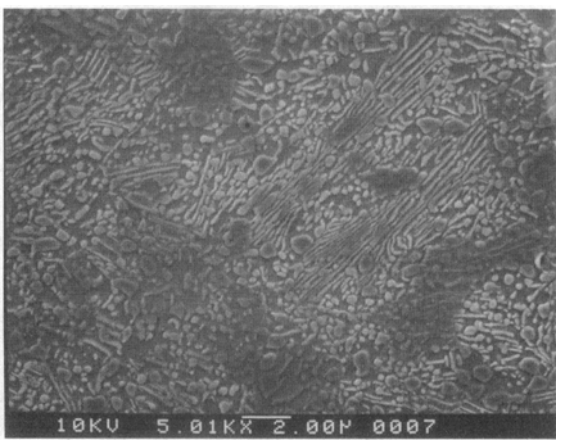

(*c*)

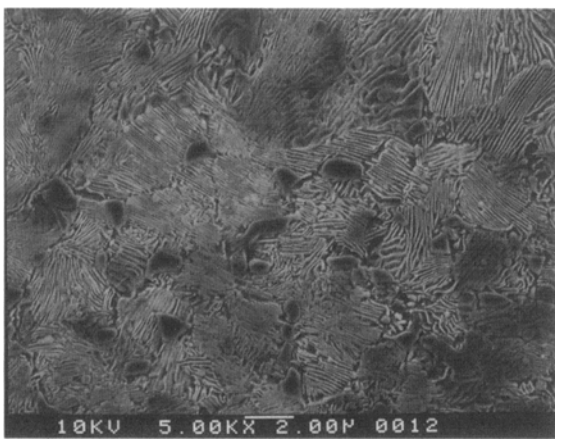

(*f*)

Fig. 2—SEM photomicrographs of the UHCS-1.5C samples transformed to pearlite after austenitizing at (*a*) 810 °C, (*b*) 840 °C, (*c*) 870 °C, (*d*) 900 °C, (*e*) 930 °C, and (*f*) 960 °C.

with the inverse square root of interlamellar spacing, as shown in Figure 7.[5,6] The data of Hyzak and Bernstein and of Gladman *et al.* show lower strengths than the UHCS materials of the present study. These differences in strength are strongly related to differences in solid solution content of the steels and will be discussed in detail later. An additional variable not considered in the analysis of data in Figure 7 is the pearlite colony size, which will also be discussed in detail later.

A comparison was made of the yield strengths of the pearlitic UHCS materials investigated here with earlier studies on the spheroidized UHCS materials. In an earlier study on spheroidized steels, the Hall–Petch relation was used to predict yield strength.[2] The prediction for yield strength was based on ferrite grain size, L, and interparticle spacing of carbide particles, D_s^*, as barriers for dislocation motion. The predictive phenomenological relation derived from these dependencies is given as

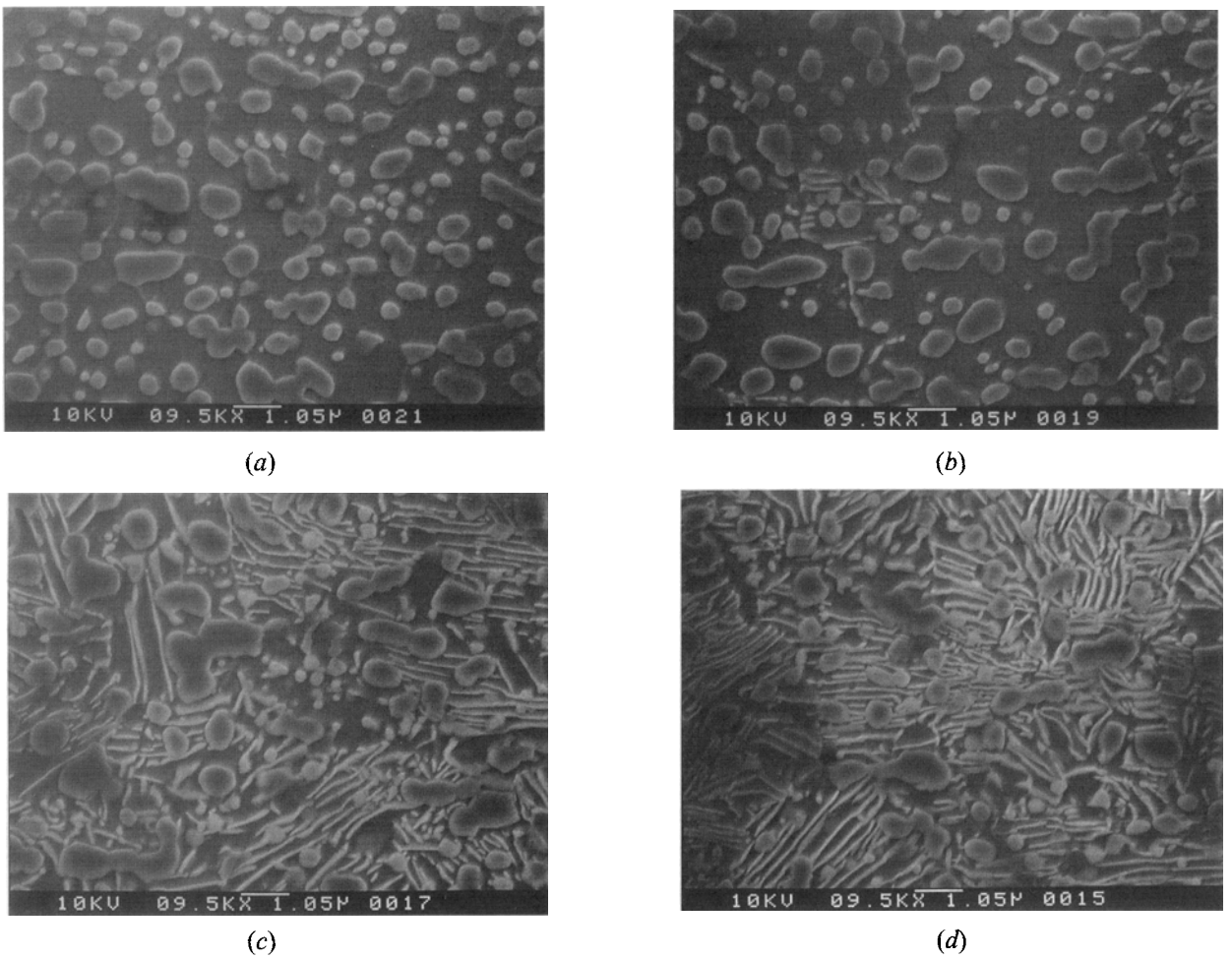

(*a*) (*b*) (*c*) (*d*)

Fig. 3—SEM photomicrographs of the UHCS-1.8C samples transformed from the (*a*) DET structure to pearlite after austenitizing at (*b*) 810 °C, (*c*) 840 °C, (*d*) 870 °C. (Parts e-f, cont. on next page)

$$\sigma_y = 310(D_s^*)^{-1/2} + 460L^{-1/2} \quad [2]$$

where lengths are in units of micrometers, and stress is in units of megapascals. In Eq. [2], the first term $(310(D_s^*)^{-1/2})$ is considered to be related to the friction stress in the Hall–Petch relation, and the second term $(460\ L^{-1/2})$ is related to the grain size term. In order to relate the microstructural parameters L and D_s^* to pearlitic microstructures, corresponding parameters were considered. The grain size, L, for a spheroidized microstructure is most logically correlated with the pearlite colony size in a pearlitic microstructure. The interparticle spacing, D_s^*, in a spheroidized microstructure should correspond to the average dislocation barrier spacing involving carbides in a pearlitic microstructure. As carbide lamella are the most obvious barriers to dislocations, the pearlite interlamellar spacing, λ, should relate to D_s^*. The average glide distance for a dislocation, however, is not equal to λ, as measured by the finest observable interlamellar spacing. This is because calculation of D_s^* from the measured value of λ in a pearlitic microstructure requires knowledge of the slip directions in the ferrite matrix between carbide lamella.

The slip directions in body-centered cubic metals are normally along the $\langle 111 \rangle$ directions.[7] If the habit plane of carbide platelets in ferrite is known, then the length along the slip direction between carbide platelets can be calculated from λ to give D_s^*. Three dominant orientation relationships have been observed between ferrite and carbide lamella in pearlitic steels of eutectoid composition.[8] These three orientation relationships between habit planes are[8–14]

$(001)_c//(11\bar{2})_f$ (Bagaryatsky)
$(103)_c//(01\bar{1})_f$ (Isaichev)
$(101)_c//(\bar{2}\bar{1}5)_f$ (Pitsch–Petch)

where the subscript of c denotes carbide orientation and the subscript of f denotes ferrite orientation. The angle between the normal of each habit plane and each of the $\langle 111 \rangle$ slip directions in ferrite, ϕ, was calculated as shown schematically in Figure 8. For each orientation relation, the angles of all slip directions which intersect the habit plane were calculated. The average of angle ϕ was then found by giving equal weight to each slip direction. The average angle from the normal to the habit plane, Φ, can be used to find the average slip distance between carbide platelets from the relation

$$D_s^* = \lambda/\cos \Phi$$

The Bagaryatsky orientation relation gives an average value for Φ of 47.7 deg, while the Isaichev and Pitsch–Petch orientation relationships give values of 56.6 and 35.3 deg, respectively. It should be noted that the measured values of these orientation relations are generally within only a few degrees of those quoted earlier.[8] For example, Zhou and

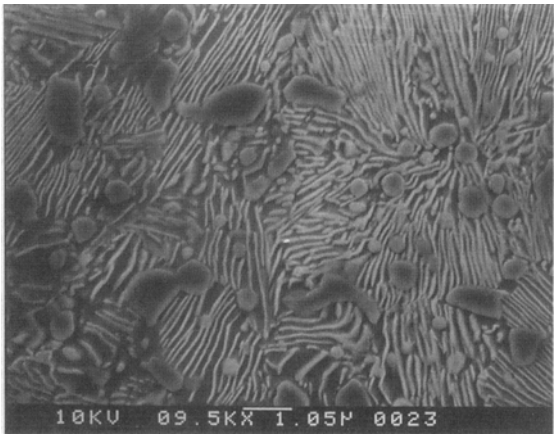

(*e*)

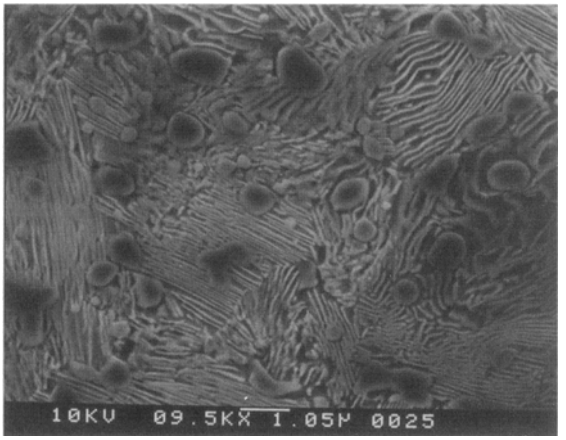

(*f*)

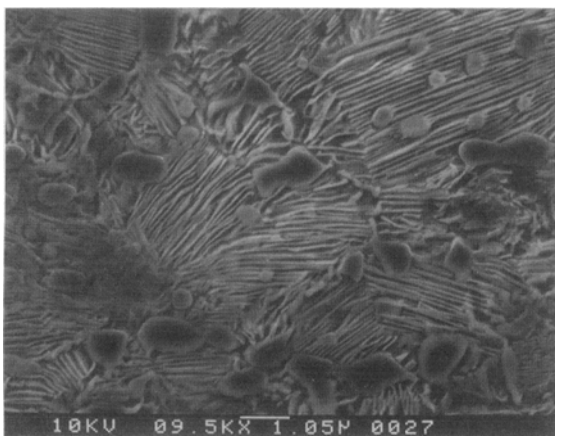

(*g*)

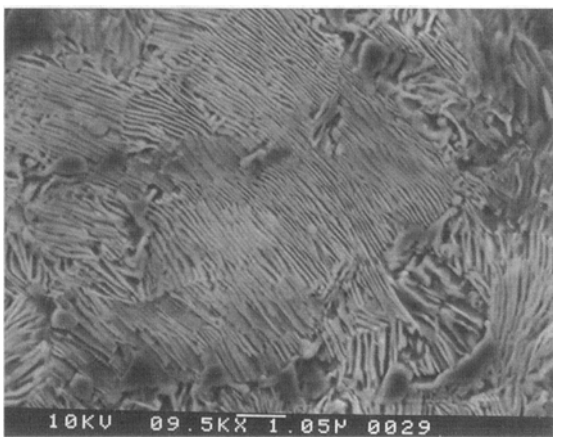

(*h*)

Fig. 3 (cont)—(*e*) 900 °C, (*f*) 930 °C, (*g*) 960 °C, and (*h*) 990 °C.

Shiflet found the measured values of the Bagaryatsky orientation relation to be always 3.8 deg from the ideal orientation given previously, a deviation which was attributed to misfit strain.[8] For this reason, Φ should be taken as accurate to within no more than approximately 5 deg. Assuming that each of the three orientation relations is of equal importance gives an average value of $\Phi = 45$ deg. Using this value yields the following relation for calculating D_s^* from the measured pearlite interlamellar spacing, λ:

$$D_s^* = \sqrt{2}\lambda \qquad [3]$$

Using this relationship for D_s^*, and values for L equal to the measured pearlite colony sizes, yield strengths were predicted using Eq. [2]. The predicted (Eq. [2]) and observed yield strengths from microstructures in which pearlite interlamellar spacings and colony sizes were measured are shown in Figure 9, which is a plot of measured yield strength *vs* predicted yield strength. Data and calculations used in this figure for the pearlitic UHCS materials are given in Table I. The data show a remarkably good fit to the predictive equation (Eq. [2]) using the same preconstants deduced from data for spheroidized hypereutectoid steels. Also shown in Figure 9 are data for a spheroidized steel of the same composition as the UHCS-1.8C in the present investigation.[2] Remarkably, both spheroidized and pearlitic microstructures fit the predictions of Eq. [2].

The predictive aspect of Eq. [2] does not explain the large strength differential between the eutectoid composition steels of other studies and the present hypereutectoid composition steels in the pearlitic condition (Figure 7). These differences are explained by taking into account the contributions of the term from Eq. [2] containing L and of solid solution alloying on the strength of pearlitic and spheroidized carbon steels. Thus, an additional term for Eq. [2] is proposed, $(\sigma_0)_{ss}$, the contribution from solid solution strengthening, which will be a constant for any given alloy composition. Equation [2] now takes the form

$$\sigma_y = (\sigma_0)_{ss} + A(D_s^*)^{-1/2} + BL^{-1/2} \qquad [4]$$

where A and B are constants to be determined from available data. While $(\sigma_0)_{ss}$ is a constant for only a particular alloy or group of alloys, the constants A and B should hold for any eutectoid or hypereutectoid steel in either spheroidized or pearlitic condition.

In order to determine the constant B of Eq. [4], it is necessary to plot yield stresses at a constant value of D_s^* against $L^{-1/2}$ and to determine the slope of the data. Data with a constant value of D_s^* are available from Syn *et al.*,[2] who made such a plot (Syn *et al.*, Figure 8) and determined that $B = 460$, which is also valid for Eq. [2]. In order to determine the constant A of Eq. [4], it is necessary to plot $(\sigma_y' - 460L^{-1/2})$ *vs* $(D_s^*)^{-1/2}$ and to measure the slope of the data. Such a plot is given in Figure 10, where A is the slope measured from data on the yield strengths of several compositional groups with pearlitic or spheroidized microstructures. The single value of slope selected was determined

Table I. The Finest Measured Pearlite Interlamellar Spacing (λ), Pearlite Colony Size (L), Measured Yield Strength (σ_y), Inverse Square Root of Interlamellar Spacing ($\lambda^{-1/2}$), and D_s^* Values for Each UHCS Material and Soaking Temperature (T) (The Standard Deviations Calculated from Microstructural Measurements Are Given)

Material	T (°C)	λ (μm)	L (μm)	σ_y (MPa)	$\lambda^{-1/2}$ ($\mu m^{-1/2}$)	D_s^* (μm)
UHCS-1.5C	840	0.18 ± 0.02	2.2 ± 0.2	864	2.36	0.25
UHCS-1.5C	870	0.18 ± 0.04	2.6 ± 0.2	889	2.36	0.25
UHCS-1.5C	900	0.13 ± 0.01	2.7 ± 0.4	950	2.77	0.18
UHCS-1.5C	930	0.11 ± 0.01	2.8 ± 0.4	1038	3.02	0.16
UHCS-1.5C	960	0.09 ± 0.01	3.6 ± 0.6	1038	3.33	0.13
UHCS-1.8C	840	0.25 ± 0.05	2.2 ± 0.4	800	2.00	0.35
UHCS-1.8C	870	0.19 ± 0.04	2.2 ± 0.2	934	2.29	0.27
UHCS-1.8C	900	0.11 ± 0.01	2.6 ± 0.6	957	3.02	0.16
UHCS-1.8C	930	0.095 ± 0.006	3.6 ± 0.9	1099	3.24	0.13
UHCS-1.8C	960	0.069 ± 0.003	4.8 ± 1.8	1204	3.81	0.10
UHCS-1.8C	990	0.065 ± 0.003	5.4 ± 3.9	1204	3.92	0.09

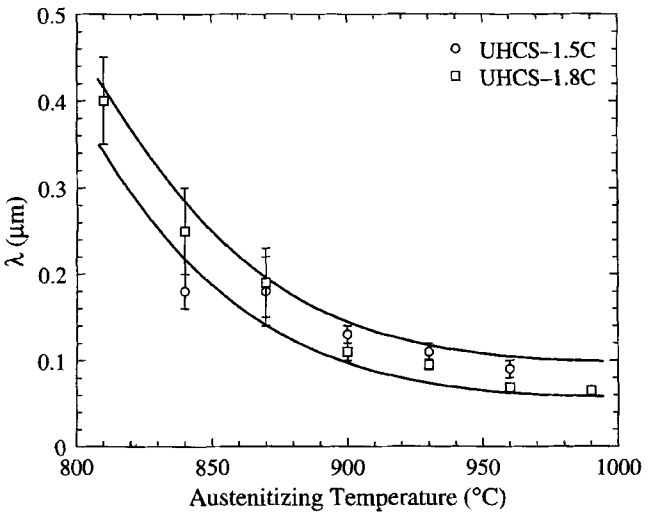

Fig. 4—Pearlite interlamellar spacing *vs* austenitizing temperature for both UHCS-1.5C and UHCS-1.8C. The value of λ given at 810 °C is the interparticle spacing.

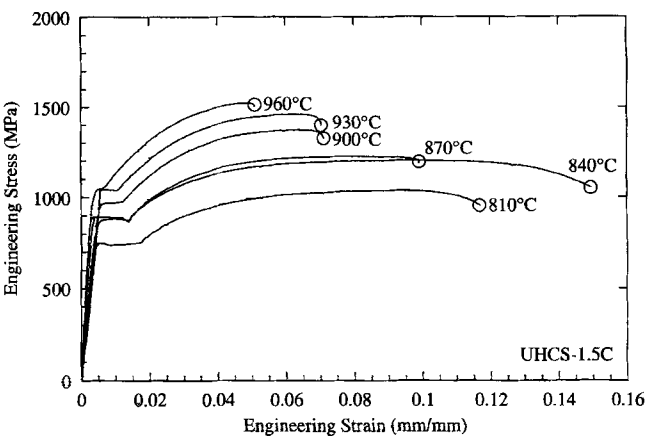

Fig. 5—Tensile test data for UHCS-1.5C at room temperature.

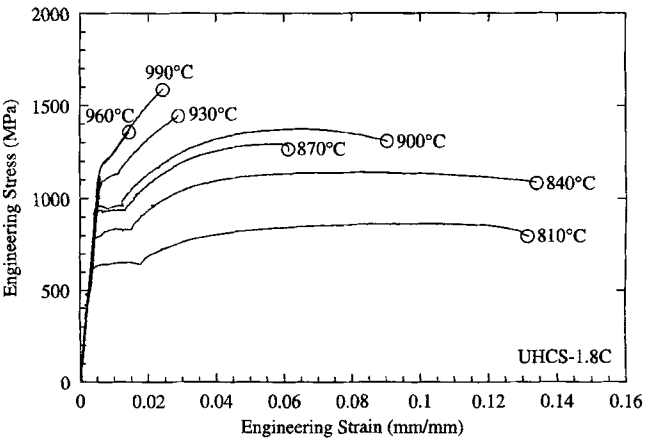

Fig. 6—Tensile test data for UHCS-1.8C at room temperature.

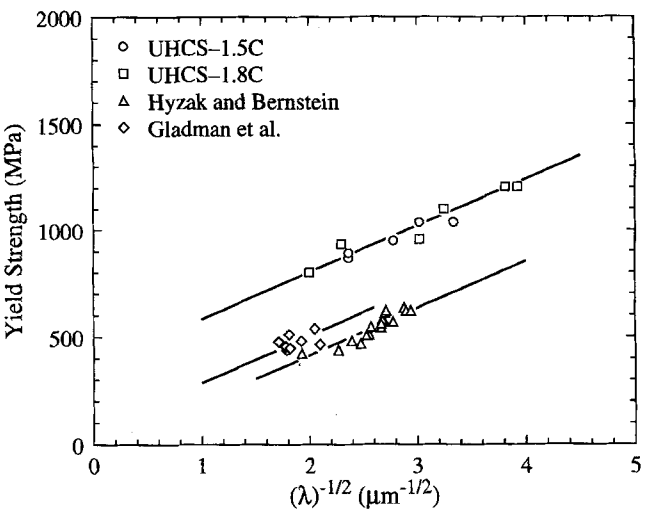

Fig. 7—Yield strength *vs* the inverse square root of pearlite interlamellar spacing for both UHCS-1.5C and UHCS-1.8C.

principally from the data for spheroidized UHCS-1.8C material giving $A = 145$. The y intercepts of the data in Figure 10 yield values of $(\sigma_0)_{ss}$ for each group of alloys, yielding the following predictive equation:

$$\sigma_y = (\sigma_0)_{ss} + 145(D_s^*)^{-1/2} + 460L^{-1/2} \quad [5]$$

The sources of the data shown in Figure 10 are listed in Table II together with the values of $(\sigma_0)_{ss}$ found from Figure 10 for each of the four alloy groups that were created based on solid solution alloy composition.

In plotting data in Figure 10, the values of L and D_s^* for the spheroidized materials were taken from those tabulated by Syn *et al.* (their Table II),[2,5,6,15–19] with the exception of data from Davidson and Ansell, where a value of $L = 16$

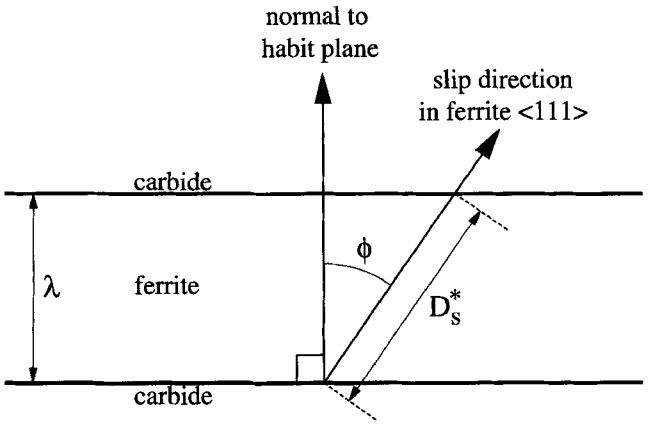

Fig. 8—Schematic showing calculations for finding D_s^* from λ using the angle ϕ.

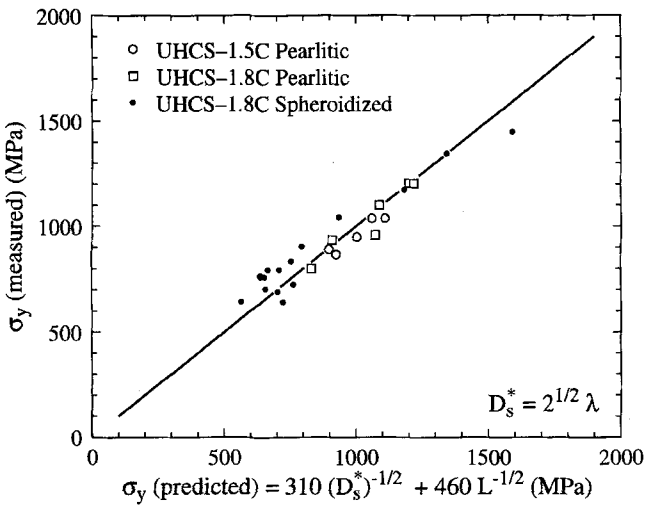

Fig. 9—Measured yield strengths *vs* predicted yield strengths from Eq. [2] for pearlitic UHCS materials and spheroidized UHCS steels. Data for spheroidized UHCS are from Ref. 2.

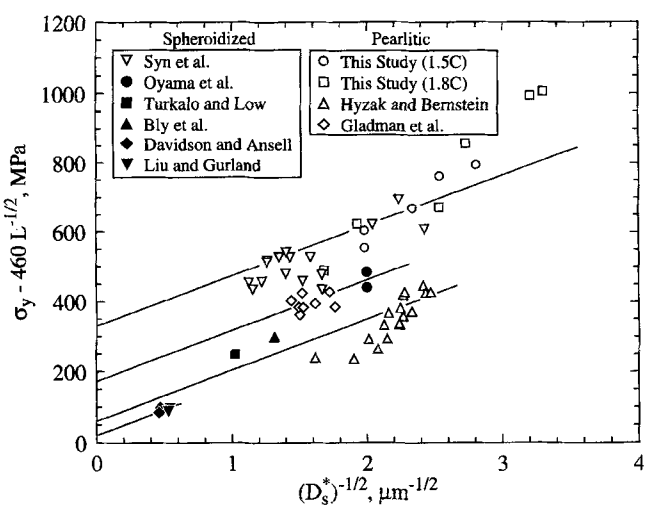

Fig. 10—Plot of $\sigma_y - 460L^{-1/2}$ *vs* $(D_s^*)^{-1/2}$ for the determination of $(\sigma_0)_{ss}$ for each of the four alloy categories. Data for spheroidized steels are from Refs. 2 and 15 through 19. Data for pearlitic steels are from this study and Refs. 5 and 6.

μm was taken from the micrograph in their Figure 2.[18] The values of L for the pearlitic steels were taken from the values given for pearlite colony size (Hyzak and Bernstein, Table II;[5] Gladman *et al.*, Table III[6]). The values for interlamellar spacing given by Hyzak and Bernstein (their Table II[5]) were used in calculating D_s^* by means of Eq. [3]. Gladman *et al.*, having used the method of Birkbeck and Wells[20] for evaluating interlamellar spacings, reported interlamellar spacing as S_0, which is not equivalent to the finest measurable interlamellar spacing reported as λ in the present investigation. Birkbeck and Wells reported the ratio of S_0 to the finest measurable interlamellar spacing to be approximately 1.3 for their data. This value of $S_0/\lambda = 1.3$ was used to convert the interlamellar spacings reported by Gladman *et al.* for calculation of D_s^* using Eq. [3].

Table II gives the composition of each alloy shown in Figure 10. The alloys in Table II are categorized into four groups, and one value of $(\sigma_0)_{ss}$ was calculated from Figure 10 for each group. These four groups are as follows:

(1) highly alloyed UHCS materials (this study; Syn *et al.*[2]), where $(\sigma_0)_{ss} = 330$ MPa;
(2) moderately alloyed UHCS and eutectoid steels (Oyama *et al.*[15] Gladman et al.[6]), where $(\sigma_0)_{ss} = 170$ MPa;
(3) low alloy eutectoid steels (Hyzak and Bernstein;[5] Turkalo and Low;[16] Bly *et al.*[17]), where $(\sigma_0)_{ss} = 60$ MPa; and
(4) unalloyed eutectoid and hypereutectoid steels (Davidson and Ansell;[18] Liu and Gurland[19]), where $(\sigma_0)_{ss} = 20$ MPa.

The highly alloyed UHCS materials give a high value for $(\sigma_0)_{ss}$ of 330 MPa, while the unalloyed eutectoid and hypereutectoid steels give a low value for $(\sigma_0)_{ss}$ of 20 MPa, which comes from solid solution strengthening by interstitial carbon. Using the $(\sigma_0)_{ss}$ values given in Table II, a predicted flow stress may be calculated from Eq. [5] for each material. In Figure 11, the predicted yield strength from Eq. [5] is compared with the measured yield strength for each material of Table II. Figure 11 shows a very good correlation of the predicted values (Eq. [5]) with the measured values over a wide range of yield strengths. The results indicate that spheroidized and pearlitic structure steels are influenced in a nearly identical manner by carbide spacing, grain size, and solid solution alloying. This is surprising since it is intuitively expected that a lamellar structure would lead to a stronger condition than a particulate structure. This expected difference is not evident from the correlations given, although a few data points for the pearlitic UHCS materials do fall above the spheroidized UHCS material in strength at fine interlamellar spacings (Figure 10).

V. CONCLUSIONS

Using the transformations in the hypereutectoid region of the Fe-C phase diagram allows for the formation of pearlitic microstructures with various interlamellar spacings and pearlite colony sizes. By varying the ratio of undissolved spheroidized carbide to pearlitic carbide, the interlamellar spacings in pearlite can be controlled to yield a range of strengths and ductilities. A phenomenological equation found to predict the yield strength for spheroidized UHCS materials based on microstructural parameters can also predict the yield strength for pearlitic UHCS materials. The microstructural parameters used to predict yield strength in

Table II. Composition in Weight Percent of Eutectoid and Hypereutectoid Steels and the Calculated Values for $(\sigma_0)_{ss}$ (Both Pearlitic (P) and Spheroidized (S) Microstructures Are Given)

Investigator	$(\sigma_0)_{ss}$ (MPa)	Method of Determination	Structure	Composition, Wt Pct							
				C	Al	Cr	Mn	Si	Ni	Cu	N
This investigation	330	Fig. 10	P	1.8	1.6	1.5	0.5	...	...	...	...
This investigation	330	Fig. 10	P	1.5	1.6	1.5	0.5	...	...	...	...
Syn *et al.*[2]	330	Fig. 10	S	1.8	1.6	1.5	0.5	...	...	...	...
Oyama *et al.*[15]	170	Fig. 10	S	1.5	...	1.5	0.5	0.5	...	...	...
Gladman *et al.*[6]	170	Fig. 10	P	0.81	...	...	0.92	0.40	...	...	0.010
	170	Fig. 10	P	0.81	...	...	0.95	0.91	...	...	0.008
	170	Fig. 10	P	0.81	...	...	1.54	0.43	...	...	0.007
	170	Fig. 10	P	0.81	...	...	1.56	0.92	...	...	0.010
	170	Fig. 10	P	0.81	...	...	0.88	0.34	...	...	0.018
	170	Fig. 10	P	0.89	...	...	0.97	0.99	...	...	0.019
	170	Fig. 10	P	0.78	...	...	1.48	0.25	...	...	0.017
	170	Fig. 10	P	0.81	...	...	1.51	0.95	...	...	0.017
Hyzak and Bernstein[5]	60	Fig. 10	P	0.81	...	...	0.87	0.17	...	...	...
Turkalo and Low[16]	60	Fig. 10	S	0.75	...	...	1.0	0.17	...	...	...
Bly *et al.*[17]	60	Fig. 10	S	0.75	...	...	0.75	0.24	0.43	0.56	...
Davidson and Ansell[18]	20	Fig. 10	S	0.83	...	...	...	...	...	...	...
	20	Fig. 10	S	1.1	...	...	...	...	...	...	...
Liu and Gurland[19]	20	Fig. 10	S	1.23	...	...	...	...	...	...	...

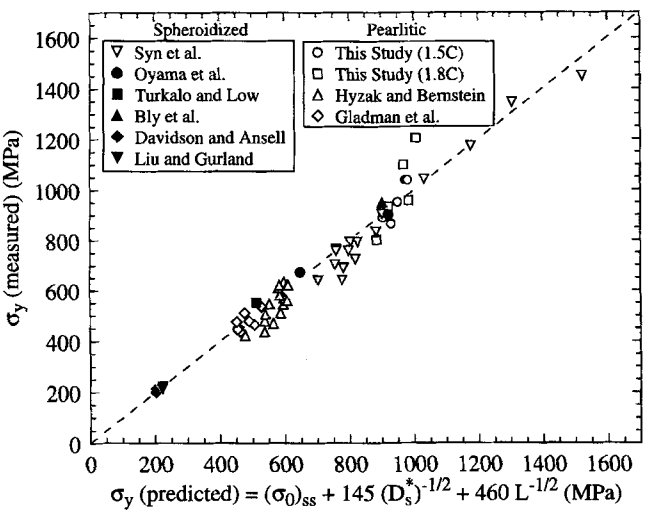

Fig. 11—Measured yield strengths *vs* predicted yield strengths from Eq. [5] for pearlitic and spheroidized hypereutectoid and eutectoid steels. Data for spheroidized steels are from Refs. 2 and 15 through 19. Data for pearlitic steels are from this study and Refs. 5 and 6.

the pearlitic microstructure steels are the pearlite colony size and the interlamellar carbide spacing. An extension of this phenomenological equation was made to account for differences in solid solution strengthening between various alloys, adding an additional parameter, $(\sigma_0)_{ss}$, which depends on alloy content. This extended analysis accurately predicts the yield strength for several pearlitic and spheroidized eutectoid and hypereutectoid steels of various alloy contents.

ACKNOWLEDGMENTS

One author (EMT) would like to express his gratitude to the Lawrence Livermore National Laboratory for assisting in the advancement of his Ph.D. thesis program at Stanford University. This work was performed under the auspices of the United States Department of Energy by the Lawrence Livermore National Laboratory, under Contract No. W-7405-ENG-48, and under the auspices of the United States Office of Naval Research by Stanford University, under Contract No. N-00014-91-J-1197.

REFERENCES

1. D.R. Lesuer, C.K. Syn, A. Goldberg, J. Wadsworth, and O.D. Sherby: *JOM*, 1993, vol. 45, pp. 40-46.
2. C.K. Syn, D.R. Lesuer, and O.D. Sherby: *Metall. Trans. A*, 1994, vol. 25A, pp. 1481-93.
3. O.D. Sherby and T. Oyama: Stanford University, Stanford, CA, unpublished research.
4. O.D. Sherby and T. Oyama: U.S. Patent No. 4,533,390, Aug. 6, 1985, pp. 1481-93.
5. J.M. Hyzak and I.M. Bernstein: *Metall. Trans. A*, 1976, vol. 7A, pp. 1217-24.
6. T. Gladman, I.D. McIvor, and F.B. Pickering: *J. Iron Steel Inst.*, 1972, vol. 210, pp. 916-30.
7. D. Hull and D.J. Bacon: *Introduction to Dislocations*, 3rd ed., Pergamon Press, New York, NY, 1984, p. 121.
8. D.S. Zhou and G.J. Shiflet: *Metall. Trans. A*, 1992, vol. 23A, pp. 1259-69.
9. I.V. Isaichev: *Zh. Tekh. Fiz.*, 1947, vol. 6, pp. 835-38.
10. Y.A. Bagaryatski: *Dokl. Akad. Nauk. SSSR*, 1950, vol. 73, pp. 1161-64.
11. N.J. Petch: *Acta Cryst.*, 1953, vol. 6, p. 96.
12. W. Pitsch: *Acta Metall.*, 1962, vol. 10, pp. 79-80.
13. H.G. Bowden and P.M. Kelly: *Acta Metall.*, 1967, vol. 15, pp. 105-11.
14. P.G. Boswell and G.A. Chadwick: *Scripta Metall.*, 1977, vol. 11, pp. 1001-02.
15. T. Oyama, U. Ritter, B. Walser, and O.D. Sherby: *Trans. Iron Steel Inst. Jpn.*, 1995, in press.
16. A.M. Turkalo and J.C. Low, Jr.: *Trans. TMS-AIME*, 1958, vol. 212, pp. 750-58.
17. D. Bly, O.D. Sherby, C. Young, and Y. Mischenkov: *Mater. Sci. Eng.*, 1973, vol. 12, pp. 41-46.
18. T.E. Davidson and G.S. Ansell: *Trans. ASM*, 1968, vol. 61, pp. 242-54.
19. C.T. Liu and J. Gurland: *Trans. TMS-AIME*, 1968, vol. 242, pp. 1535-42.
20. G. Birkbeck and T.C. Wells: *Trans. AIME*, 1968, vol. 242, pp. 2217-20.